Received <day> <Month>, <year>; | Revised <day> <Month>, <year>; | Accepted <day> <Month>, <year>

DOI: xxx/xxxx

ARTICLE TYPE

Reference Raman Spectrum and Mapping of *Cryptosporidium parvum* Oocysts

Dmitry Malyshev[1] | Tobias Dahlberg[1] | Rasmus Öberg[1] | Lars Landström[2] | Magnus Andersson*[1,3]

[1]Department of Physics, Umeå University, Umeå, Sweden
[2]Swedish Defence Research Agency (FOI), Umeå, Sweden
[3]Umeå Centre for Microbial Research (UCMR), Umeå, Sweden

Correspondence
*Magnus Andersson, Department of Physics, Umeå University, Umeå, Sweden, 90187. Email: magnus.andersson@umu.se

Abstract

Cryptosporidium parvum is a protozoan parasite and among the most infectious diarrhea-causing pathogens, leading to severe health problems for malnourished children and immunocompromised individuals. Outbreaks are common even in developed countries, originating from water or food contamination and resulting in suffering and large costs for society. Therefore, robust, fast and highly specific detection strategies of *Cryptosporidium* are needed. Label-free detection techniques such as Raman spectroscopy have been suggested, however high-resolution reported spectra in the literature are limited. In this work, we report reference Raman spectra at 3 cm^{-1} resolution for viable and inactivated *Cryptosporidium* oocysts of the species *C. parvum*, gathered at a single oocyst level using a laser tweezers Raman spectroscopy system. We furthermore provide tentative Raman peak assignments for the *Cryptosporidium* oocysts, along with Raman mapping of the oocysts' heterogeneous internal structure. Finally, we compare the *C. parvum* Raman spectrum with other common enterotoxigenic pathogens: *Escherichia coli*, *Vibrio cholerae*, *Bacillus cereus* and *Clostridium difficile*. Our results show a significant difference between *C. parvum* Raman spectra and the other pathogens.

KEYWORDS:
Vibrio cholerae; Clostridium difficile; Escherichia coli; Bacillus cereus; laser tweezers Raman spectroscopy

1 | INTRODUCTION

Cryptosporidium is a genus of waterborne pathogenic protozoan parasites that cause a severe gastrointestinal disease called cryptosporidiosis[1]. Both humans and animals can be infected, and of particular note are the species that commonly infect humans, *Cryptosporidium parvum* (*C. parvum*) and *Cryptosporidium hominis* (*C. hominis*)[2]. Infection can happen through person-to-person contact, animal-to-person contact, or via ingestion of contaminated food or water[3]. Cryptosporidiosis is one of the most common waterborne diseases and one of the common causes of death among young children (48 000 cases in 2016)[4]. Outbreaks occur globally, resulting in >12 million disability-adjusted life-years[4] with high costs for society[5,6]. One of *Cryptosporidium*'s strengths as a pathogen is its ability to form resilient oocysts, which are 5 μm in diameter spherical particles. See SEM images of *C. parvum* oocysts in Figure 1 and Figure S1. Oocysts are non-motile and can remain infective outside the host for over one year[7]. Each oocyst contains four sporozoites that infect the epithelial cells in the intestine and ingesting as few as ten oocysts can be sufficient to cause infection in humans[8,9].

Oocysts can be inactivated with high doses of UV radiation [10]; however, they are highly resistant to chemical decontamination techniques. Ethanol, as well as commonly used chlorine solutions, including bleach, do not kill *Cryptosporidium* oocysts [7]. The suggested protocol for decontaminating water is 5-6 % hydrogen peroxide for 20 minutes [11,12]. Boiling water, as well as drying the oocysts for more than 4 hours are also effective decontamination methods, but these methods are not practical in treating larger water sources like water reservoirs or swimming pools [11]. If the decontamination is unsuccessful and a person is infected, the resulting cryptosporidiosis gives similar symptoms as bacterial gastrointestinal pathogens. Bacteria-related diarrhea is often successfully treated using antibiotics; however, *Cryptosporidium* are strongly resistant to most antibiotics since they are not prokaryotes. A misdiagnosis of cryptosporidiosis as a bacterial infection leads to an ineffective antibiotic treatment, which increases mortality and contributes to the evolution of antibiotic-resistant bacteria [13]. Therefore, robust, swift and highly specific methods to detect *Cryptosporidium* in contaminated water and fecal matter are needed.

Currently, the most widespread technique for detecting *Cryptosporidium* oocysts in water samples is based on fluorescence microscopy in which a sampling step is needed. The oocysts are then separated from the water and other contaminants using specialized filters, after which they are stained with antibody-conjugated fluorescent dyes and detected in a fluorescence microscope. Other conventional methods employ immunological and polymerase chain reaction techniques for detecting oocysts [14,15]. Although there is room for improved efficiency of these methods, for example, by utilizing autofluorescence from the oocysts, these methods in their current form suffer from drawbacks such as being labor-intensive, having high costs, and long detection times.

An alternative label-free and highly specific detection method of biological and chemical content is Raman spectroscopy. Raman scattering approaches provide advantages over other spectroscopic techniques such as IR, since Raman signals are generally not affected by the presence of water and Raman bands are much narrower and thus easier to identify than fluorescence bands [16,17]. Raman spectroscopy, therefore, provides good possibilities for accurate chemical fingerprinting *Cryptosporidium*. However, normal Raman signals are often significantly weaker than fluorescence signals, which can be problematic for rapid detection as it implies long integration times. To improve Raman signals, surface-enhanced Raman spectroscopy (SERS) has been suggested for *Cryptosporidium* detection [18,19]. However, SERS approaches usually adds to the complexity of both system set up and spectral response compared to normal Raman. Furthermore, SERS only gives a strong signal enhancement in close adjacency to the signal enhancing structure. Therefore, only the chemical content of the outer surface is enhanced, making oocysts identification difficult and easily masked by other organic material that can be attached to its surface. Normal Raman is therefore simpler to use, however, to our knowledge there is currently no high-spectral resolution reference Raman spectrum of *Cryptosporidium* in the literature. Also, there is a lack of a *Cryptosporidium* oocysts Raman map that provides spatial information of the structure. Accurate, high resolution reference spectra are critical for reducing false alarms in classification/identification algorithms.

In this work, we present Raman spectra of both viable and neutralized *C. parvum* oocysts, captured by a Laser Tweezers Raman Spectroscopy instrument (LTRS). We also perform Raman mapping to illustrate the spatial distribution of individual components in the oocyst. Finally, we compare the Raman spectral signature with those of other common gastrointestinal pathogens to assess the possibilities to discriminate between pathogens.

2 | MATERIALS AND METHODS

2.1 | Experimental setup and measurement procedure

To trap oocysts and acquire Raman spectra we used our LTRS instrument that is custom-built in an inverted microscope (IX71, Olympus) [20,21], with the schematic of the system shown in Figure 2 . We used a Gaussian laser beam operating at 785 nm (Cobolt 08-NLD) that is coupled into the microscope using a dichroic shortpass mirror with a cut-off wavelength of 650 nm (DMSP650, Thorlabs). Imaging and focusing of the beam was achieved by a 60× water immersion objective (UPlanSApo60xWIR, Olympus) with a numerical aperture of 1.2 and a working distance of 0.28 mm. The same laser was used for Raman light excitation. In general, we operated the laser at fixed output power of 100 mW corresponding to a power of about 60 mW in the sample (total energy of 1.2 J when exposed for 20 seconds).

We collected the backscattered light by the microscope objective and passed it through a notch filter (NF785-33, Thorlabs) to reduce the Rayleigh scattered laser line. Further, to increase the signal-to-noise ratio, we have mounted a 150 μm diameter pinhole in the focal point of the telescope. The filtered light is coupled into our spectrometer (Model 207, McPherson) through a 150 μm wide entrance slit where a 600 grooves/mm holographic grating disperses the light [22]. The Raman spectrum was then

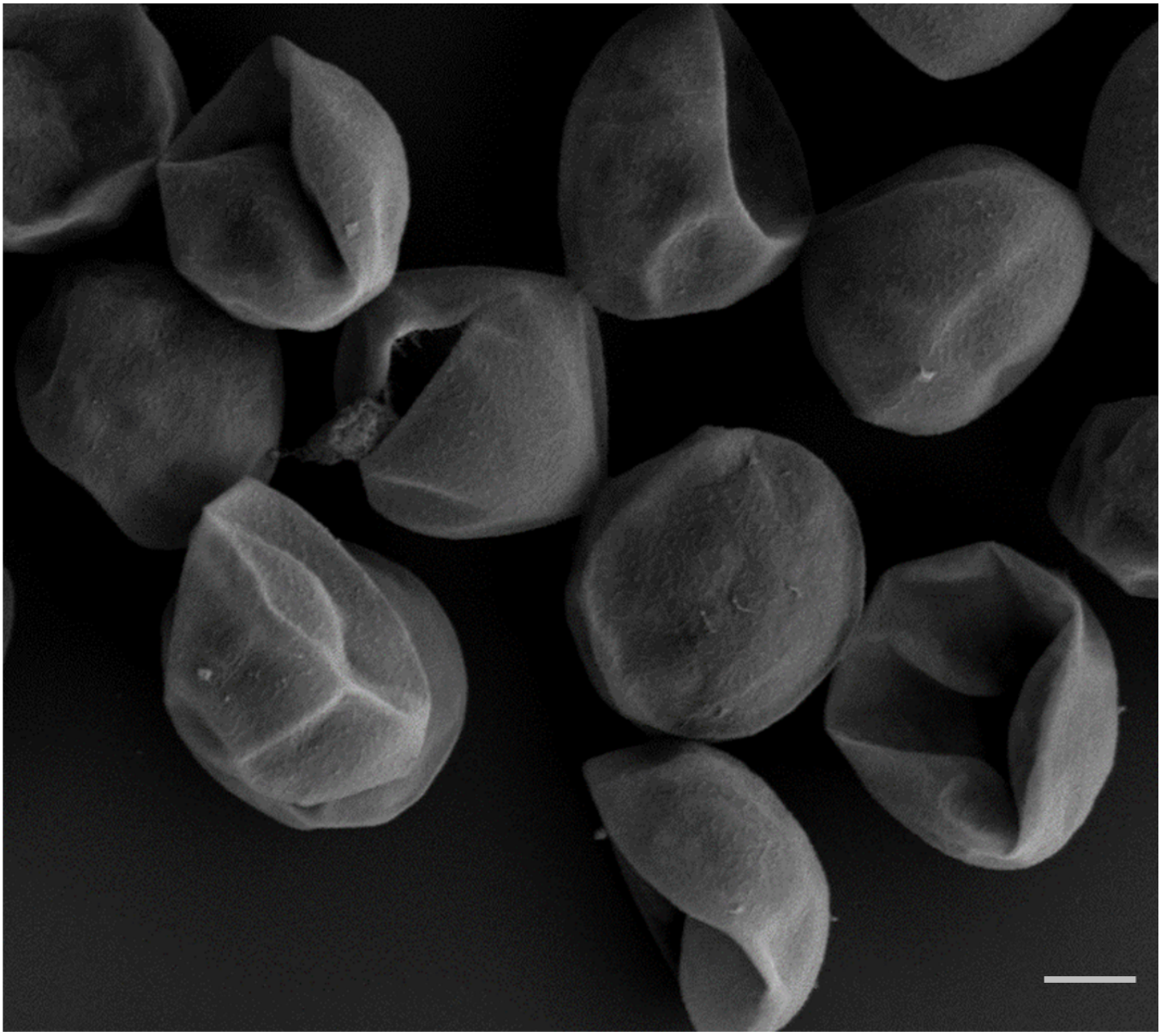

FIGURE 1 SEM image of *C. parvum* oocysts. Scale bar is 1 μm.

captured using a Peltier cooled CCD detector (Newton 920N-BR-DDXW-RECR, Andor) operated at -95° C. Our system has a Raman wavenumber spectral resolution of < 3 cm^{-1} and accuracy of ~ 3 cm^{-1}.

2.2 | Strains, culture media, and conditions

We used oocysts of the species *Cryptosporidium parvum* (Iowa isolate), aged one to two months when measured (Waterborne Inc, New Orleans). The supplied oocysts were harvested from infected calves, extracted from feces with diethyl ether and purified using percoll density gradient centrifugation. Viable oocysts were stored in PBS, with penicillin, streptomycin, gentamicin, amphotericin B and 0.01 % polysorbate 20. Neutralized oocysts were stored in PBS with 5 % Formalin and 0.01 % polysorbate 20. Stocks were stored at 4° C. To purify and remove storage solution, oocysts were washed twice by centrifuging at 3000 rcf for 2 min, with sterile water, with the supernatant discarded.

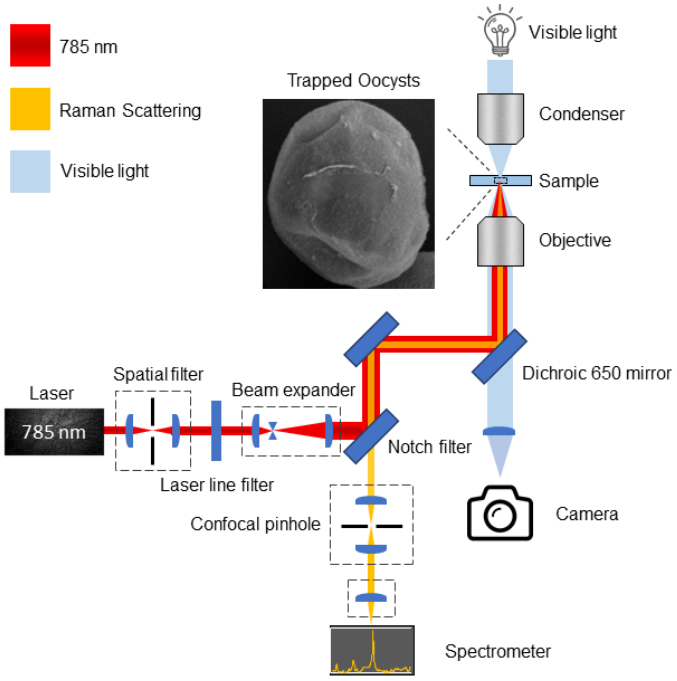

FIGURE 2 Schematic of the laser tweezer/Raman system used.

We used *Vibrio cholerae* (*V. cholerae*) str. *'El Tor'* clinical isolates N16961[23]. These bacteria were provided by Felipe Cava (Umeå university). We grew bacteria using standard laboratory conditions. Cultures were streaked onto LB plates with 200 µg mL^{-1} streptomycin, and single colonies are selected and grown overnight in TG Broth (5 g L^{-1} Tryptone, 10 g L^{-1} NaCl, 5 % glycerol) at 30 °C and sub-cultured in fresh TG Broth before measurement.

We grew *Escherichia coli* (*E. coli*) HB101/pHMG93 cells using LA plates supplemented with 100 μg ml^{-1} kanamycin at 37° C for 24 h[24].

Clostridium difficile (*C. difficile*) DS1813 spores were provided by Les Baillie (Cardiff University). Spores were grown on BHIS agar at 37 ° C for 4 days. The cells were collected, left overnight to sporulate, and then purified using density gradient centrifugation in 50 % sucrose as described previously[25]. Spores were then washed in deionised water and stored at 4° C.

Wild type *Bacillus cereus* (*B. cereus*) strain NVH 0075-95 spores were provided by Marina Aspholm (Norwegian University of Life Sciences) and stored at 4° C. For the preparation of these see reference[26].

2.3 | Sample preparation and reference spectrum acquisition

We prepared a sample by placing a 1 cm diameter ring of 1 mm thick vacuum grease on a 24 mm × 60 mm glass coverslip. We added 5 μl of the oocyst suspension into the ring, after which we sealed it by placing a 23 mm × 23 mm glass coverslip on top. After the sample was placed in the LTRS instrument, we measured the Raman spectra using 2 accumulations of 10 seconds for spores and oocysts, and using 2 accumulation of 90 seconds for bacterial cells. We measured on 100 individual oocysts each for both viable and neutralized oocysts and averaged the spectra.

2.4 | Data processing and analysis for reference spectra

We used an open-source Matlab script provided by the Vibrational Spectroscopy Core Facility at Umeå University to process Raman spectra[27]. To baseline correct the spectra we used an asymmetrical least-squares algorithm[28] with $\lambda = 10^4$ and $p = 10^{-3}$. We smoothed spectra using a Savitzky-Golay filter[29] of polynomial order 1 and a frame rate of 5. Graphs were plotted in Origin 2018 (OriginLab).

2.5 | Raman mapping

To perform Raman mapping, we placed 5 μl of the oocyst suspension in water between two 0.25 mm thick quartz coverslips (Alfa Aesar), separated by a 1 mm PDMS ring. We then find a settled oocyst and take sequential measurements of the Raman spectrum starting from the top left and moving in 1 μm steps using the piezo stage (PI-P5613CD, Physik Instruments), for a final mapping area of 5 μm by 4 μm (30 pixels per oocyst). We performed two accumulations at each location to cover the same spectral range of 600 - 1780 cm^{-1} as in other measurements. We measured on five individual oocysts.

To create Raman maps, we processed spectra into a map using an in-house Matlab script. In the script, we began by background-correcting the spectra in two steps. First, we subtracted a measured background spectrum. Next, we removed any residual background using asymmetric least-squares[28]. We then smoothed the corrected spectra using Savitzky-Golay filtering. Intensities of relevant spectral peaks (943, 1005, and 1443 cm^{-1}) provided pixel intensity values which were processed by a 2D linear interpolation of the intensities and their spatial coordinates. Next, we normalized the resulting interpolants between 0 and 1 with respect to their maximum and minimum values. Finally, we plotted the interpolated intensity as a color map on top of a brightfield image of the mapped oocyst.

2.6 | SEM imaging of Oocysts

To perform SEM imaging, we dehydrated the oocysts in series of graded ethanol solutions, starting with 50 % ethanol, and subsequent washes in 70 %, 80 %, 90 %, and 100 % ethanol. We then placed a suspension drop on the glass slide, and let it dry. We then coated the sample with a ∼5 nm layer of platinum using a Quorum Q150T-ES sputter coater. We imaged samples by a Carl Zeiss Merlin FESEM electron microscope using InLens imaging mode at magnifications in the range of 15,000 - 50,000×.

3 | RESULTS AND DISCUSSION

3.1 | Raman spectra of viable and neutralized *C. parvum*

Since *C. parvum* oocysts are spherical objects of ~ 5 μm diameter, they are clearly observed in brightfield microscopy. With the LTRS instrument we can thereby trap a single *C. parvum* oocyst and acquire a Raman spectrum. Oocysts can be trapped and moved in three dimensions using only 2.5 mW of laser power (reducing to approximately 1.5 mW in the sample), indicating that they have a rather high index of refraction for light at 785 nm. However, we used 60 mW of laser power and integrated the collected Raman scattered light for 20 seconds over Raman wavenumber 600 - 1780 cm^{-1}. The short integration time at this power did not affect the appearance of an oocyst in the microscope nor the acquired Raman spectrum, indicating no thermal damage, which is of importance to consider since a high dose might damage the trapped object[30]. In total, we measured $n = 100$ viable and neutralized oocysts respectively, and averaged their spectra into representative graphs as shown in Figure 3 . The high resolution of our experimental setup shows that oocyst spectra consist of several distinct Raman peaks.

Average Raman spectra of both viable and neutralized oocysts are very similar with no prominent peaks unique to either sample once the background is subtracted, however, a small peak at 1211 cm^{-1} is present among the neutralized oocysts but not the viable ones. Some relative peak intensities are different between neautralized and viable average spectra, with peaks of 867, 943, 1005, 1086 and 1270 cm^{-1} more prominent for neutralized oocysts, while the peak of 1301 cm^{-1} is more prominent for viable oocysts. There is support in published studies that oocysts treated with formalin have their surface chemically altered[31] and this can explain the difference in Raman spectra. We suggest more studies aimed at assessing the impact of chemicals on oocysts Raman spectra since this is an unexplored field. For example, by trapping oocysts in an LTRS instrument and exposing them to chemicals, one can measure changes and shifts of Raman peaks with time. These experiments can provide relevant information on the chemicals' mode of action on oocysts, similarly to what has been done on bacterial spores[32]. In addition, volume mapping using confocal Raman can provide more details of how sporozoites are organized inside the oocysts.

A tentative assignment of the major peaks is given in Table 1. Raman spectra of the oocysts show peaks associated with amino acids and fatty acids, which is within expectation for the oocysts. In particular, the reported Raman spectra of oleic acid[33] and the related phospholipid phosphatidylcholine shows strong similarity to the oocyst spectra. The reported peaks for phosphatidylcholine are at 719, 1088, 1270, 1301, 1442 and 1660 cm^{-1} [34] which closely matches the measured peaks of the oocysts. Phosphatidylcholine was previously reported to be the predominant lipid in the oocysts[35] which is consistent with our Raman data. Another study failed to find detectable amounts of phosphatidylcholine in the oocyst walls[36], which indicates that the phospholipid is within the oocyst, and not the walls. Two more Raman peaks from the oocyst, situated at 872 and 943

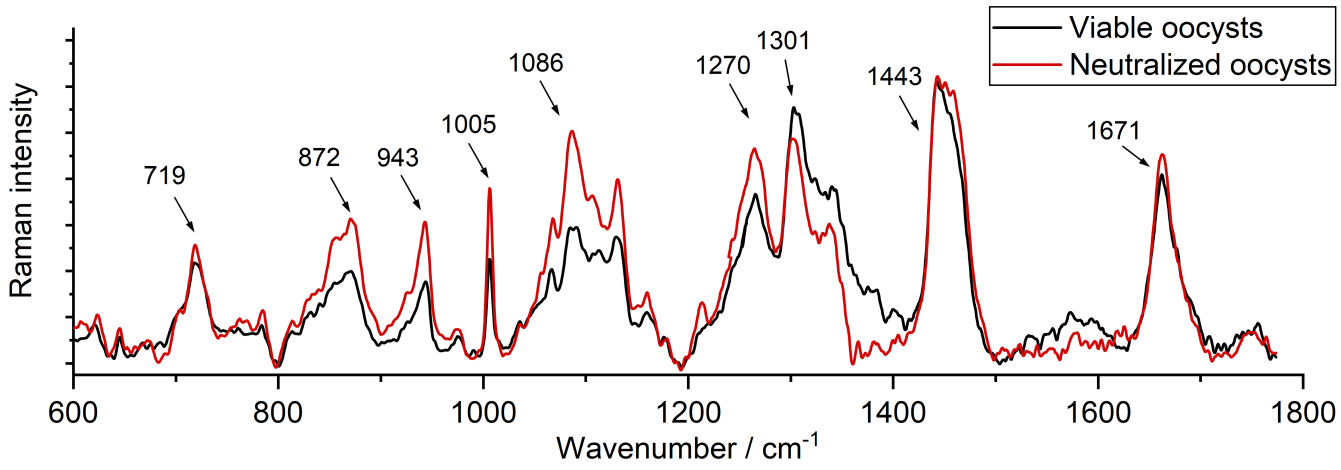

FIGURE 3 Raman spectrum of viable (black) and neutralized (red) *C. parvum* oocysts. Each spectrum is an average of spectra from 100 individual oocysts and the background has been subtracted.

TABLE 1 Peak positions and tentative assignments of selected Raman bands of *C. parvum* oocysts

Peak position	Tentative Assignment	Reference
719	Phospholipid, Adenine	[34,40]
872	Tryptophan, Galactosamine	[37,38]
943	Proline, Valine, Galactosamine	[37,38]
1005	Phenylalanine	[40]
1086	Phospholipid	[34,40]
1270	Phospholipid: Amide III	[34,40]
1301	Phospholipid	[34,40]
1443	Phospholipid	[34,40]
1671	Phospholipid: Amide I	[34,40]

cm^{-1}, are characteristic of several prevalent amino acids such as tryptophan, proline, and valine[37]. They also correspond well to the sharp Raman peaks found from galactosamine[38]. The presence of galactosamine in *Cryptosporidium* oocysts is further mentioned in a study by Stein *et al.* where the authors suggest that galactosamine is present on the surface of *Cryptosporidium* oocysts, aiding the oocyst in binding to host cells[39]. Finally, the strong 1005 cm^{-1} peak likely corresponds to phenylalanine[40].

When trapping oocysts and measuring a Raman spectrum, we noted that oocysts were orientated differently in the trap and that peak intensities varied within the population. We hypothesised that different orientations of oocysts and peak variations originated from trapping a non-homogeneous large object, as indicated in Figure 4 A. Since oocysts are much larger than the beam waist of the laser used for Raman spectroscopy ($\sim 5\ \mu$m compared to 400 nm beam waist), we only take a spectrum of a small region with a measurement, which can contribute to the variation seen between samples. To resolve this variation, we Raman mapped oocysts with 1 μm resolution, sampling 30 pixels. A representative Raman mapping measurement of an oocyst illustrating the intensity distribution of three different Raman bands, is seen in Figure 4 B-D. All five Raman mapped occysts are shown in Figure S2. The results show heterogeneity in the intensity distribution of the different Raman peaks, which has overlaps with structures that are visible in the brightfield image. We speculate that these structures may be the sporozoites, as these would have a different chemical composition than the rest of the oocyst content. The heterogeneity is likely caused by the different viewing angles at which the sporozoites are observed and their location in the oocyst. Since the sporozoites are only $4 \times 0.6\ \mu$m[41], there are many possible ways they can fit into the oocyst.

We were not able to identify any peaks corresponding to unique oocyst wall components, for example, specific fatty acids, hydrocarbons and fatty alcohols, as reported by Jenkins *et al.*[31]. However, their concentration may be too low to resolve from

other fatty acids, hydrocarbons and fatty alcohols predominant in the oocysts. Also, the Raman spectra of individual fatty acids have significant overlap[33], so it is not possible to resolve these as the signal from phosphatidylcholine masks the others.

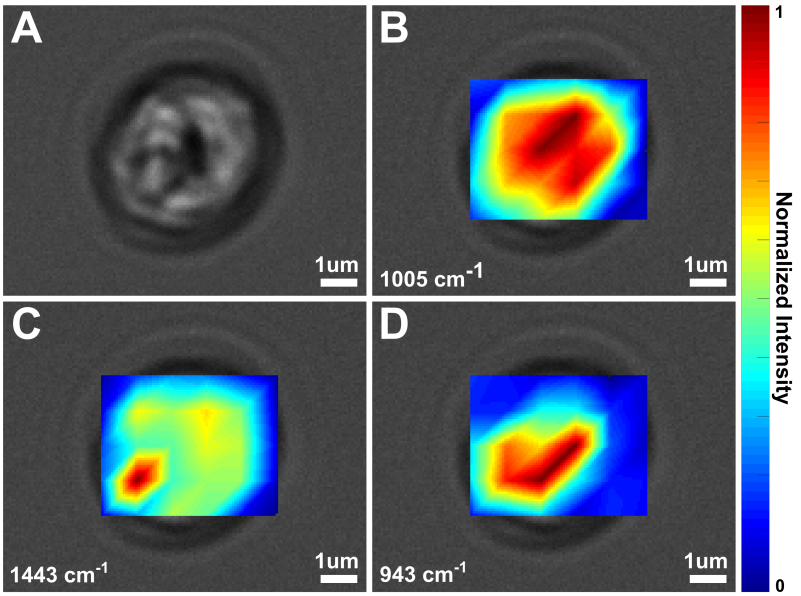

FIGURE 4 Brightfield image and Raman mapping of *C. parvum*. Raman mapping was performed by moving the focal point of the laser with 1 μm steps in the horizontal and 1 μm steps in the vertical direction, respectively. Color intensity corresponds to relative peak intensity. A) a brightfield image of an oocysts. Raman map overlay of the B) 1443 cm^{-1} peak, C) 1005 cm^{-1}, and D) 943 cm^{-1}.

3.2 | Raman spectra of oocysts are distinct from spectra of other gastrointestinal pathogens

Many microbial pathogens cause acute gastrointestinal disease, the second most common cause of death of children up to 5 years in developing countries[42]. *C. parvum* belong to this group together with pathogens such as enterotoxigenic *E. coli*, and *V. cholerae*. In addition, strains of *B. cereus* and *C. difficile* are two common food-borne pathogens causing diarrheal disease[43,44]. Identifying the causing pathogen is vital in an outbreak when choosing the right disinfection method and theraputic approach to diarrheal disease, as well as to minimize the outbreak itself. For *Cryptosporidium* this is of particular interest since these infections give similar symptoms as enterotoxigenic *E. coli* and *V. cholerae* which are treated using antibiotics (for example, tetracycline and fluoroquinolones). However, nitazoxanide is the only FDA approved anti-parasitic treatment for *Cryptosporidium* infections[45]. Thus, it is very important to have a robust detection method that can discriminate between pathogens to use the right disinfection approach and to know what pathogen to treat for when a person is infected.

To investigate if it is possible to robustly distinguish the Raman signal from *C. parvum* with *E. coli*, *V. cholerae*, *B. cereus*, *C. difficile* we also performed single cell Raman measurements on these pathogens. Representative SEM images of each pathogen are shown in Figures S1, and S3 - S6. Since it is known that the cell wall composition, as well as the inner cell of these pathogens are different, we anticipated that the Raman signals should reflect these differences at the single-cell level. For example, as mentioned above, the biochemical composition of the oocyst cell wall structure consists of carbohydrate components, medium and long fatty acids, proteins, and aliphatic hydrocarbons[36]. In comparison, the cell wall of *E. coli* cells are mainly lipid-rich, and contain a peptidoglycan layer further into the cell[46]. For *B. cereus* and *C. difficile* we measured the spectra of spores, the state they are often found in the environment. In spores, the outer layers are protein and peptidoglycan rich, whereas the inner layers consist of up to 25 % CaDPA, a common spore biomarker[47].

In Figure 5 we show Raman spectra of these pathogens alongside the spectrum from *C. parvum* oocysts. We observe that the Raman spectra of the oocysts differ greatly from those of other non-oocyst pathogens. The most prominent Raman peaks

of spore pathogens *B. cereus* and *C. difficile* occur at 1017 cm^{-1} in close conjunction with a smaller peak at 1001 cm^{-1}. These two peaks are characteristic peaks of CaDPA. Although these peaks are comparable in appearance to the sharp peak of the *Cryptosporidium* oocyst appearing at 1005 cm^{-1}, the oocysts are clearly distinguishable from the spore pathogens by their lack of prevalent Raman peaks at 660 and 825 cm^{-1}, as well as their significant activity between 1050 - 1350 cm^{-1}. Comparing the Raman spectrum of the oocysts to those of *V. cholerae* and *E. coli*, we similarly observe prominent peaks around 1000 cm^{-1}. Unlike the spore pathogens but similarly to *C. parvum*, *V. cholerae* and *E. coli* exhibit active Raman spectra with several broad peaks around 1100 and 1250 cm^{-1}. The two can, however, be distinguished from *C. parvum* by their prevalent peak characteristic of DNA and situated around 780 cm^{-1}, which is largely obscured in the Raman spectrum of *C. parvum*. The Raman peaks of *C. parvum* are also significantly more intense in the 1200-1800 cm^{-1}, likely due to the larger amount of phospholipid compared to the cell.

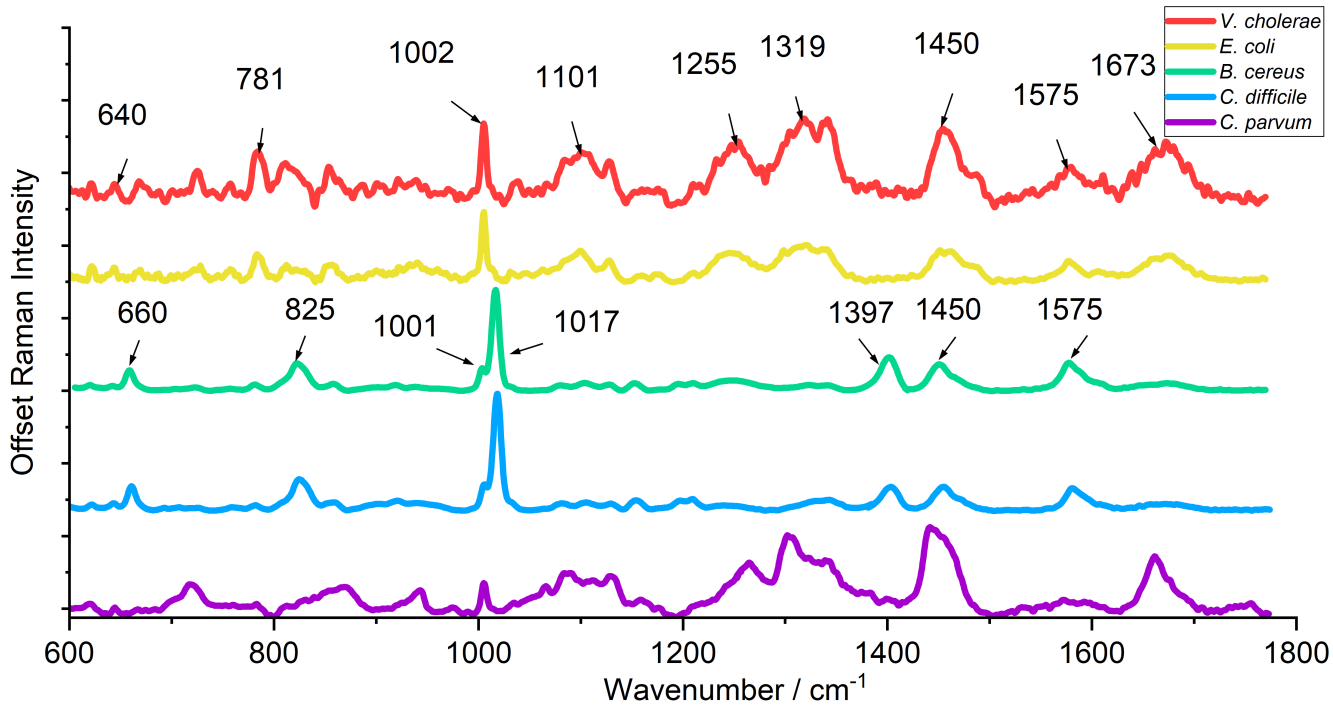

FIGURE 5 Normalized Raman spectra comparison of *V. cholerae* cells (red), *E. coli* cells (yellow), *B. cereus* spores, (green) *C. difficile* spores (blue) and *C. parvum* oocysts (purple). The spectra of vegetative cells, oocysts and spores are clearly distinct from each other, while the spore spectra are very similar. An average of at least ten samples were used for each spectra.

4 | CONCLUSIONS

Cryptosporidium infections are problematic for humans and animals, resulting in suffering and high costs for society. As symptoms are similar to other enterotoxic pathogens, specific and fast identification of *Cryptosporidium* oocysts is important for using the correct disinfection method and to ordinate the most suitable therapeutic. To assess if normal Raman spectroscopy is suitable to fingerprint oocysts and if their spectra can easily be discriminated from other common enterotoxic pathogens, we measured Raman spectra of single *C. parvum* oocysts using an LTRS instrument. Our results show that spectra of *C. parvum* oocysts are indeed different than those of *V. cholerae* and *E. coli* cells, as well as *B. cereus* and *C. difficile* spores. The Raman signals of viable and formalin neutralized oocysts were however largely similar. We also carried out peak assignment of oocysts and identified phosphatidylcholine as one of the major contributors to the Raman spectrum. Our Raman mapping shows that phosphatidylcholine is distributed throughout the oocyst apart from the walls, while amino acid-associated peaks are more localised,

to a part of any given oocyst, which we believe is the location of the sporozoites. Thus, we conclude that Raman spectroscopy can be used to detect the presence of oocysts in water and that the unique oocysts fingerprint can easily be differentiated from other common gastrointestinal pathogens.

5 | ACKNOWLEDGEMENTS

We thank Felipe Cava, Les Baillie, and Marina Aspholm for providing bacterial strains. We thank Oihane Irazoqui for making SEM images of *V. cholerae*. This work was supported by the Swedish Research Council (2019-04016); the Umeå University Industrial Doctoral School (IDS); Kempestiftelserna (JCK-1916.2); Swedish Department of Defence (A74028).

The authors acknowledge the facilities and technical assistance of the Umeå Core Facility for Electron Microscopy (UCEM) at the Chemical Biological Centre (KBC), Umeå University, a part of the National Microscopy Infrastructure NMI (VR-RFI 2016-00968)

References

1. Riggs MW, Perryman LE. Infectivity and neutralization of Cryptosporidium parvum sporozoites. *Infection and Immunity* 1987; 55(9): 2081–2087. doi: 10.1128/iai.55.9.2081-2087.1987

2. Bouzid M, Hunter PR, Chalmers RM, Tyler KM. Cryptosporidium Pathogenicity and Virulence. *Clinical Microbiology Reviews* 2013; 26(1): 115–134. doi: 10.1128/CMR.00076-12

3. Efstratiou A, Ongerth JE, Karanis P. Waterborne transmission of protozoan parasites: Review of worldwide outbreaks - An update 2011–2016. *Water Research* 2017; 114: 14–22. doi: 10.1016/j.watres.2017.01.036

4. Khalil IA, Troeger C, Rao PC, et al. Morbidity, mortality, and long-term consequences associated with diarrhoea from Cryptosporidium infection in children younger than 5 years: a meta-analyses study. *The Lancet Global Health* 2018; 6(7): e758–e768. doi: 10.1016/S2214-109X(18)30283-3

5. Chyzheuskaya A, Cormican M, Srivinas R, et al. Economic assessment of waterborne outbreak of cryptosporidiosis. *Emerging Infectious Diseases* 2017; 23(10): 1650–1656. doi: 10.3201/eid2310.152037

6. Guy RA, Yanta CA, Muchaal PK, et al. Molecular characterization of Cryptosporidium isolates from humans in Ontario, Canada. *Parasites & Vectors* 2021; 14(1): 69. doi: 10.1186/s13071-020-04546-9

7. Chen F, Huang K, Qin S, Zhao Y, Pan C. Comparison of viability and infectivity of Cryptosporidium parvum oocysts stored in potassium dichromate solution and chlorinated tap water. *Veterinary Parasitology* 2007; 150(1-2): 13–17. doi: 10.1016/j.vetpar.2007.09.001

8. Current WL, Garcia LS. Cryptosporidiosis. *Clinics in Laboratory Medicine* 1991; 11(4): 873–897. doi: 10.1016/S0272-2712(18)30525-0

9. Okhuysen PC, Chappell CL, Sterling CR, Dupont HL. Virulence of three distinct C. parvum isolates in healthy adults. *Clinical Infectious Diseases* 1997; 25(2): 428.

10. Adeyemo FE, Singh G, Reddy P, Bux F, Stenström TA. Efficiency of chlorine and UV in the inactivation of Cryptosporidium and Giardia in wastewater. *PLOS ONE* 2019; 14(5): e0216040. doi: 10.1371/journal.pone.0216040

11. Bogan JE. Disinfection Techniques for Cryptosporidium. *Journal of Dairy & Veterinary Sciences* 2018; 7(4): 1–3. doi: 10.19080/JDVS.2018.07.555718

12. Weir SC, Pokorny NJ, Carreno RA, Trevors JT, Lee H. Efficacy of common laboratory disinfectants on the infectivity of Cryptosporidium parvum oocysts in cell culture. *Applied and Environmental Microbiology* 2002; 68(5): 2576–2579. doi: 10.1128/AEM.68.5.2576-2579.2002

13. Arslan AH, Ciloglu FU, Yilmaz U, Simsek E, Aydin O. Discrimination of waterborne pathogens, Cryptosporidium parvum oocysts and bacteria using surface-enhanced Raman spectroscopy coupled with principal component analysis and hierarchical clustering. *Spectrochimica Acta Part A: Molecular and Biomolecular Spectroscopy* 2022; 267: 120475. doi: 10.1016/j.saa.2021.120475

14. Luka G, Samiei E, Dehghani S, Johnson T, Najjaran H, Hoorfar M. Label-Free Capacitive Biosensor for Detection of Cryptosporidium. *Sensors* 2019; 19(2): 258. doi: 10.3390/s19020258

15. Hassan EM, Örmeci B, DeRosa MC, Dixon BR, Sattar SA, Iqbal A. A review of Cryptosporidium spp. And their detection in water. *Water Science and Technology* 2021; 83(1): 1–25. doi: 10.2166/wst.2020.515

16. MacCarthy P, Rice JA. Spectroscopic methods (other than NMR) for determining functionality in humic substances.. *Humic substances in soil, sediment, and water. Geochemistry, isolation, and characterization* 1985(April): 527–559.

17. Wei D, Chen S, Liu Q. Review of Fluorescence Suppression Techniques in Raman Spectroscopy. *Applied Spectroscopy Reviews* 2015; 50(5): 387–406. doi: 10.1080/05704928.2014.999936

18. Rule K, Vikesland PJ. Surface-enhanced resonance raman spectroscopy for the rapid detection of cryptosporidium parvum and giardia lamblia. *Environmental Science and Technology* 2009; 43(4): 1147–1152. doi: 10.1021/es801531t

19. Luka G, Samiei E, Tasnim N, Dalili A, Najjaran H, Hoorfar M. Comprehensive review of conventional and state-of-the-art detection methods of Cryptosporidium. *Journal of Hazardous Materials* 2022; 421(February 2021): 126714. doi: 10.1016/j.jhazmat.2021.126714

20. Stangner T, Dahlberg T, Svenmarker P, et al. Cooke–Triplet tweezers: more compact, robust, and efficient optical tweezers. *Optics Letters* 2018; 43(9): 1990. doi: 10.1364/ol.43.001990

21. Dahlberg T, Malyshev D, Andersson PO, Andersson M. Biophysical fingerprinting of single bacterial spores using laser Raman optical tweezers. In: Guicheteau JA, Howle CR., eds. *Chemical, Biological, Radiological, Nuclear, and Explosives (CBRNE) Sensing XXI*SPIE; 2020: 28

22. Dahlberg T, Andersson M. Optical design for laser tweezers Raman spectroscopy setups for increased sensitivity and flexible spatial detection. *Applied Optics* 2021; 60(16): 4519. doi: 10.1364/AO.424595

23. Heidelberg JF, Elsen JA, Nelson WC, et al. DNA sequence of both chromosomes of the cholera pathogen Vibrio cholerae. *Nature* 2000; 406(6795): 477–483. doi: 10.1038/35020000

24. Goransson M, Forsman K, Uhlin BE. Regulatory genes in the thermoregulation of Escherichia coli pili gene transcription.. *Genes & Development* 1989; 3(1): 123–130. doi: 10.1101/gad.3.1.123

25. Malyshev D, Williams CF, Lees J, Baillie L, Porch A. Model of microwave effects on bacterial spores. *Journal of Applied Physics* 2019; 125(12). doi: 10.1063/1.5085442

26. Pradhan B, Liedtke J, Sleutel M, et al. Endospore Appendages: a novel pilus superfamily from the endospores of pathogenic Bacilli. *The EMBO Journal* 2021: 1–16. doi: 10.15252/embj.2020106887

27. Vibrational spectroscopy core facility, https://www.umu.se/en/research/infrastructure/visp/downloads/, accessed 22-01-27.

28. Eilers PHC. Parametric Time Warping. *Analytical Chemistry* 2004; 76(2): 404–411. doi: 10.1021/ac034800e

29. Savitzky, A.; Golay MJE. Smoothing and Differentiation. *Anal. Chem* 1964; 36(8): 1627–1639.

30. Malyshev D, Öberg R, Dahlberg T, et al. Laser induced degradation of bacterial spores during micro-Raman spectroscopy. *Spectrochimica Acta Part A: Molecular and Biomolecular Spectroscopy* 2022; 265: 120381. doi: 10.1016/j.saa.2021.120381

31. Jenkins MB, Eaglesham BS, Anthony LC, Kachlany SC, Bowman DD, Ghiorse WC. Significance of wall structure, macromolecular composition, and surface polymers to the survival and transport of Cryptosporidium parvum oocysts. *Applied and Environmental Microbiology* 2010; 76(6): 1926–1934. doi: 10.1128/AEM.02295-09

32. Malyshev D, Dahlberg T, Wiklund K, Andersson PO, Henriksson S, Andersson M. Mode of Action of Disinfection Chemicals on the Bacterial Spore Structure and Their Raman Spectra. *Analytical Chemistry* 2021; 93(6): 3146–3153. doi: 10.1021/acs.analchem.0c04519

33. Matuszyk E, Sierka E, Rodewald M, et al. Differential response of liver sinusoidal endothelial cells and hepatocytes to oleic and palmitic acid revealed by Raman and CARS imaging. *Biochimica et Biophysica Acta - Molecular Basis of Disease* 2020; 1866(6): 165763. doi: 10.1016/j.bbadis.2020.165763

34. Pezzotti G. Raman spectroscopy in cell biology and microbiology. *Journal of Raman Spectroscopy* 2021; 52(12): 2348–2443. doi: 10.1002/jrs.6204

35. Mitschler RR, Welti R, Upton SJ. A Comparative Study of Lipid Compositions of Cryptosporidium parvum (Apicomplexa) and Madin-Darby Bovine Kidney Cells. *The Journal of Eukaryotic Microbiology* 1994; 41(1): 8–12. doi: 10.1111/j.1550-7408.1994.tb05927.x

36. Jenkins MB, Eaglesham BS, Anthony LC, Kachlany SC, Bowman DD, Ghiorse WC. Significance of Wall Structure, Macromolecular Composition, and Surface Polymers to the Survival and Transport of Cryptosporidium parvum Oocysts. *Applied and Environmental Microbiology* 2010; 76(6): 1926–1934. doi: 10.1128/AEM.02295-09

37. Qiu S, Li M, Liu J, et al. Study on the chemodrug-induced effect in nasopharyngeal carcinoma cells using laser tweezer Raman spectroscopy. *Biomedical Optics Express* 2020; 11(4): 1819. doi: 10.1364/BOE.388785

38. De Gelder J, Scheldeman P, Leus K, et al. Raman spectroscopic study of bacterial endospores. *Analytical and Bioanalytical Chemistry* 2007; 389(7-8): 2143–2151. doi: 10.1007/s00216-007-1616-1

39. Stein B, Stover L, Gillem A, Winters K, Lee JH, Chauret C. The effect of lectins on Cryptosporidium parvum oocyst in vitro attachment to host cells. *Journal of Parasitology* 2006; 92(1): 1–9. doi: 10.1645/GE-570R.1

40. Maquelin K, Kirschner C, Choo-Smith LP, et al. Identification of medically relevant microorganisms by vibrational spectroscopy. *Journal of Microbiological Methods* 2002; 51(3): 255–271. doi: 10.1016/S0167-7012(02)00127-6

41. Leitch GJ, He Q. Cryptosporidiosis-an overview. *Journal of Biomedical Research* 2012; 25(1): 1–16. doi: 10.1016/S1674-8301(11)60001-8

42. Liu L, Oza S, Hogan D, et al. Global, regional, and national causes of under-5 mortality in 2000–15: an updated systematic analysis with implications for the Sustainable Development Goals. *The Lancet* 2016; 388(10063): 3027–3035. doi: 10.1016/S0140-6736(16)31593-8

43. Qadri F, Svennerholm AM, Faruque aSG, Sack RB. Enterotoxigenic Escherichia coli in developing countries: epidemiology, microbiology, clinical features, treatment, and prevention.. *Clinical microbiology reviews* 2005; 18(3): 465–83. doi: 10.1128/CMR.18.3.465-483.2005

44. Kouhsari E, Abbasian S, Sedighi M, et al. Clostridium difficile infection: A review. *Reviews in Medical Microbiology* 2018; 29(3): 103–109. doi: 10.1097/MRM.0000000000000135

45. Anderson RV, Curran PM. Nitazoxanide. *Drugs* 2007; 67(13): 1947–1967.

46. Silhavy TJ, Kahne D, Walker S. The bacterial cell envelope. *Cold Spring Harbor perspectives in biology* 2010; 2(5): a000414. doi: 10.1101/cshperspect.a000414

47. Zhang X, Young MA, Lyandres O, Van Duyne RP. Rapid Detection of an Anthrax Biomarker by Surface-Enhanced Raman Spectroscopy. *Journal of the American Chemical Society* 2005; 127(12): 4484–4489. doi: 10.1021/ja043623b

Reference Raman Spectrum and Mapping of *Cryptosporidium parvum* Oocysts

Dmitry Malyshev[1], Tobias Dahlberg[1], Rasmus Öberg[1], Lars Landström[2], and Magnus Andersson[1,3,*]

[1]Department of Physics, Umeå University, Umeå, Sweden
[2]Swedish Defence Research Agency (FOI), Umeå, Sweden
[3]Umeå Center for Microbial Research (UCMR), Umeå, Sweden

*Corresponding author Magnus Andersson
Email: magnus.andersson@umu.se
Phone:+46 90 786 6336

Supplementary Methods

SEM imaging of bacterial cells

To perform SEM imaging of cells, we first harvested bacterial cells and fixate them in 2% paraformaldehyde for 15 min at room temperature. Fixed samples were then cast onto poly-L-lysine coated glass slides and dehydrated in series of graded ethanol (70, 80, 90, 95, 100%).Then, they were critical point dried and coated with an iridium layer of 5 nm using a Quorum Q150T-ES sputter coater. We examined samples by Carl Zeiss Merlin FESEM electron microscope using InLens imaging mode.

SEM imaging of spores

To perform SEM imaging of spores, we air dried a 5 µl drop of spore suspension on a glass slide. We then coat the sample with a ~5 nm layer of platinum and examined as described above.

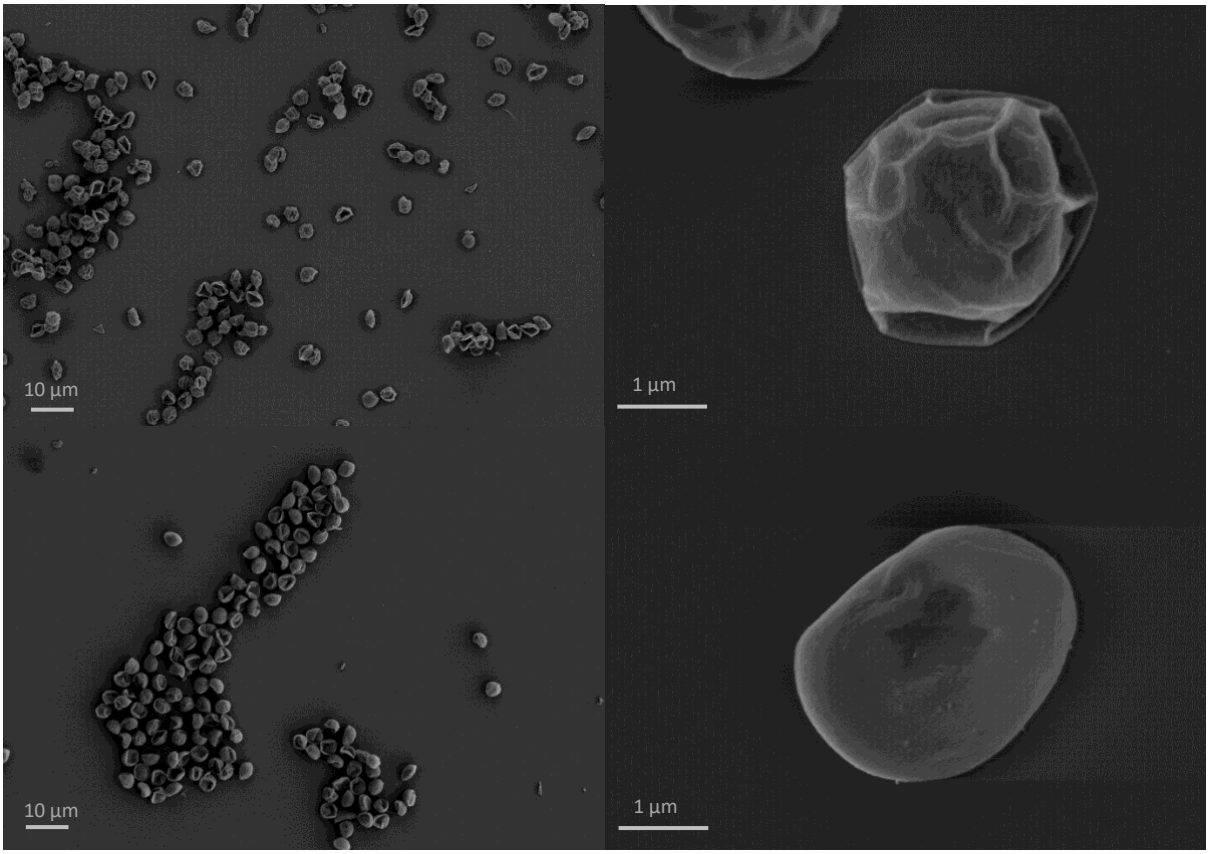

Figure S1. SEM micrographs of *C. parvum* oocysts at different resolution.

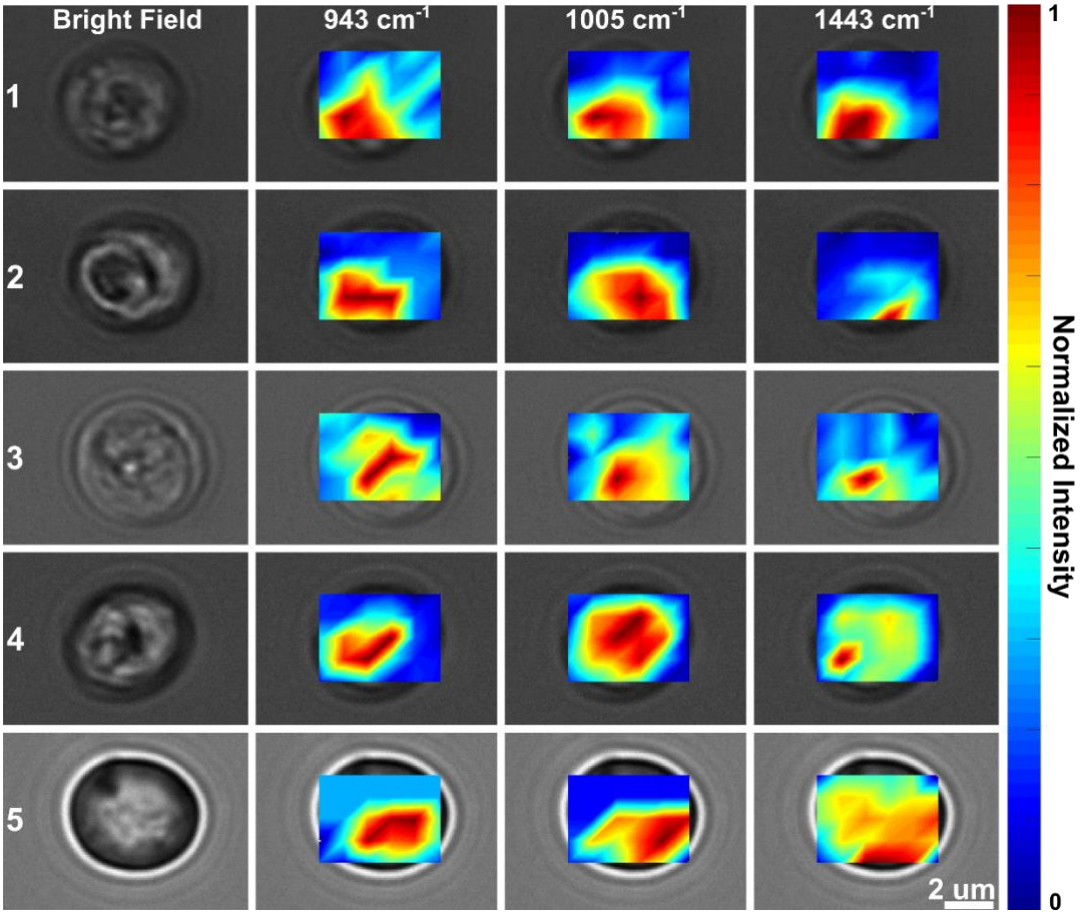

Figure S2. Raman mapped oocysts.

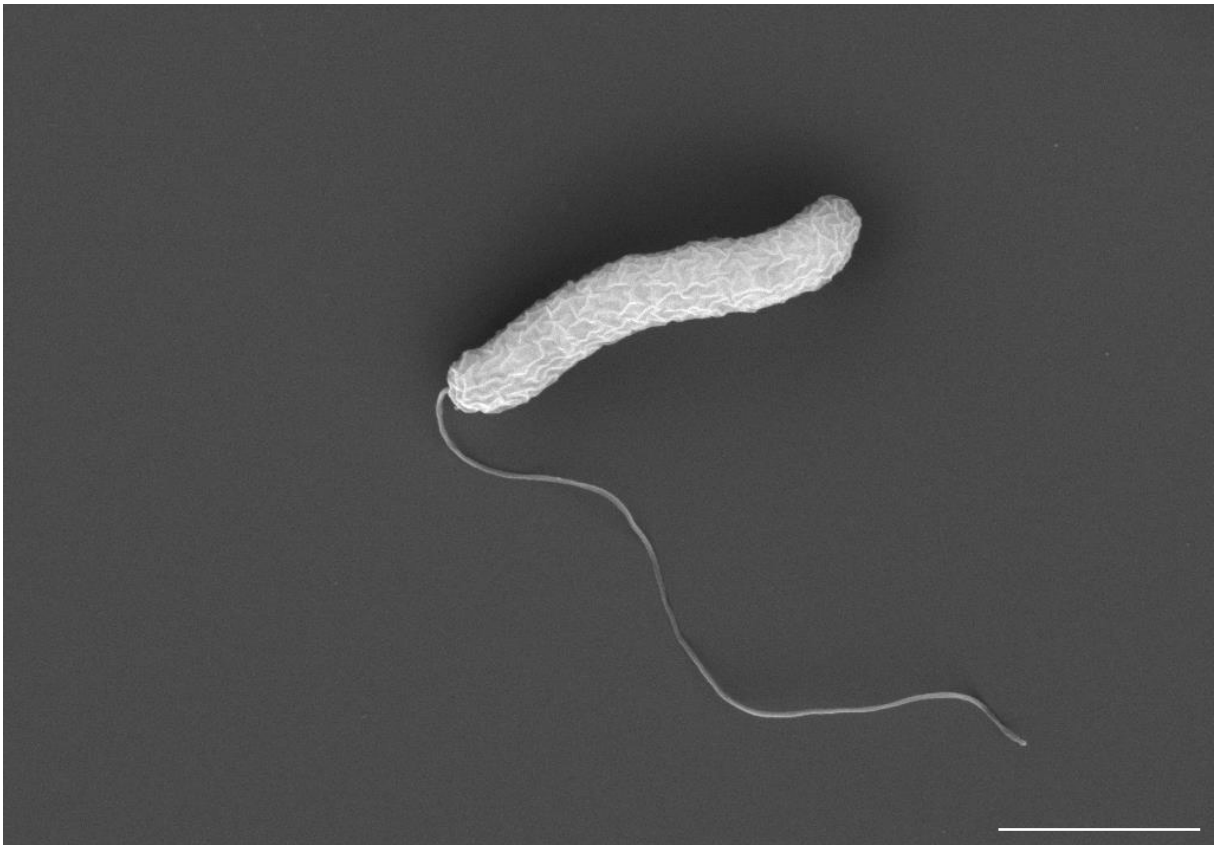

Figure S3. SEM micrograph of *V. cholerea* bacterium. Scalebar is 1 µm.

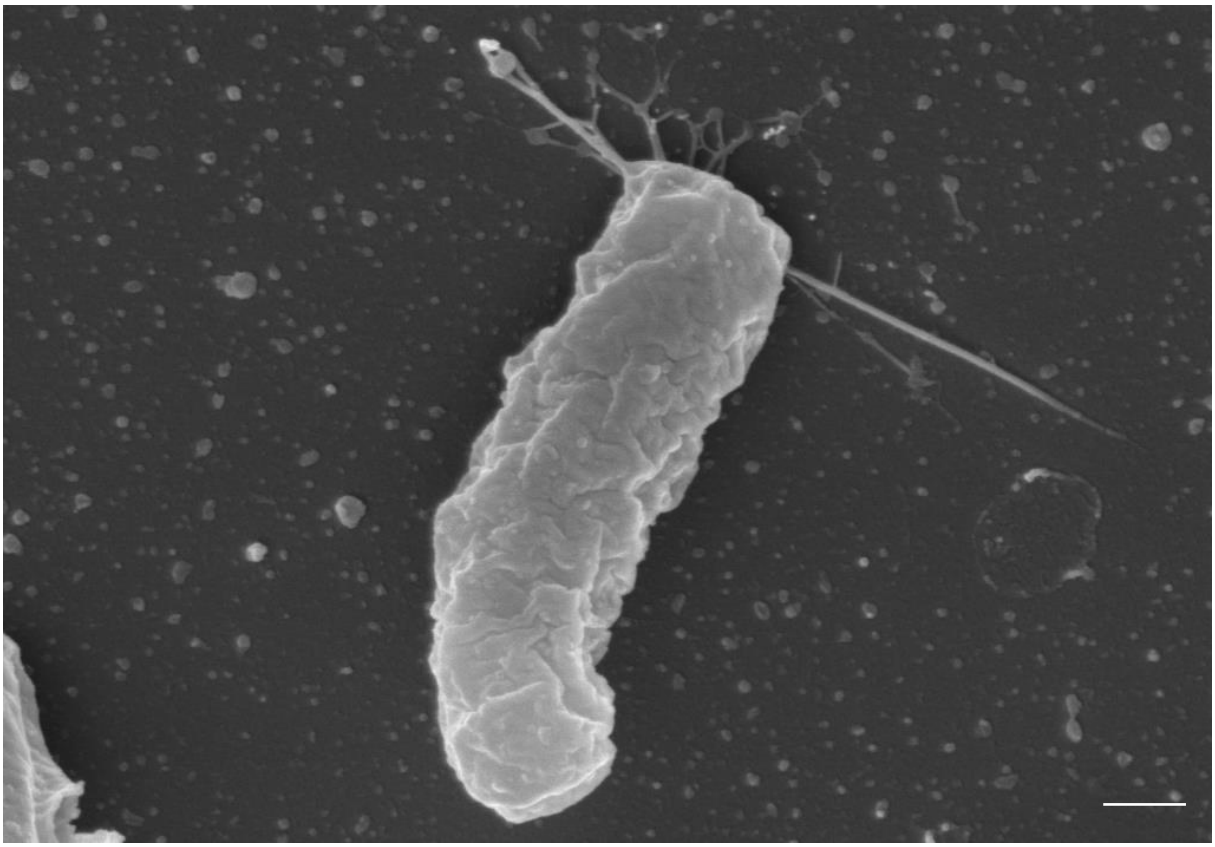

Figure S4. SEM micrograph of *E. coli* bacterium. Scalebar is 200 nm.

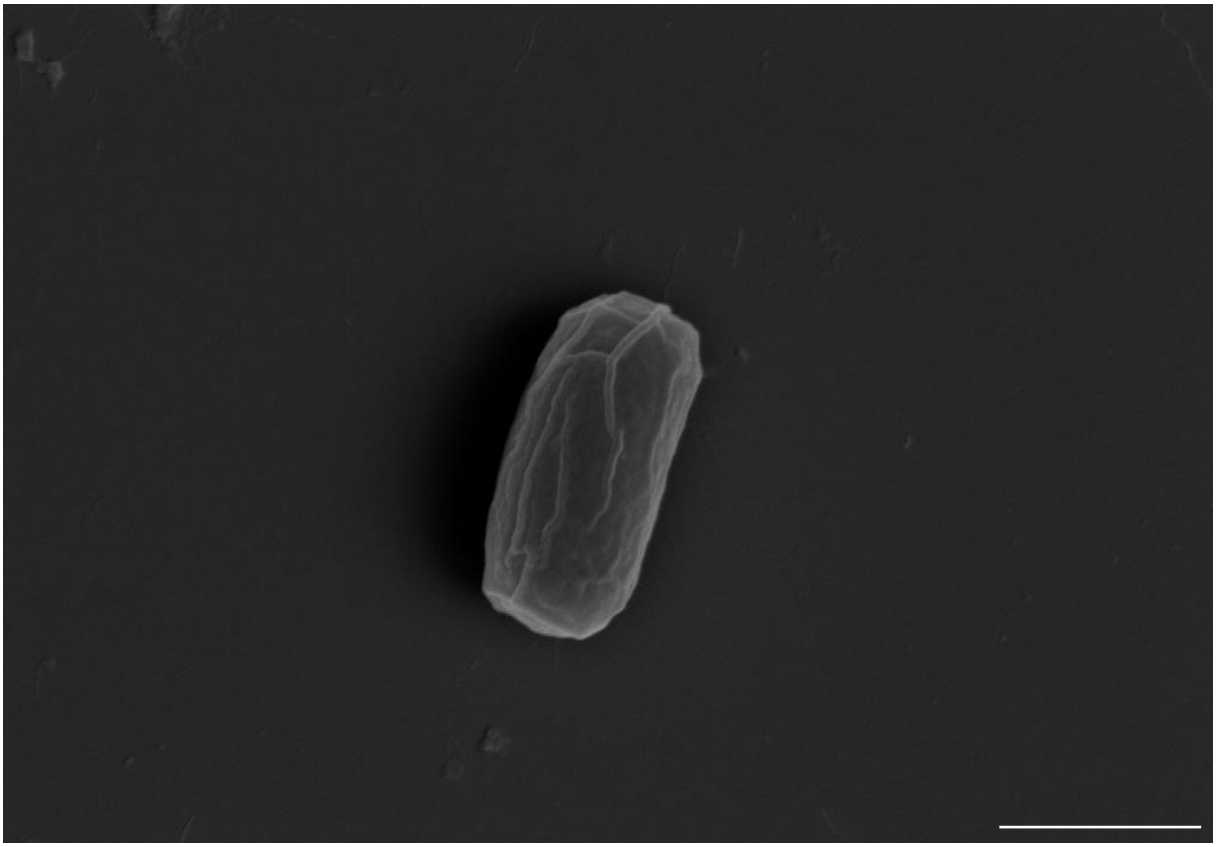

Figure S5. SEM micrograph of *B. cereus* spore. Scalebar is 1 µm.

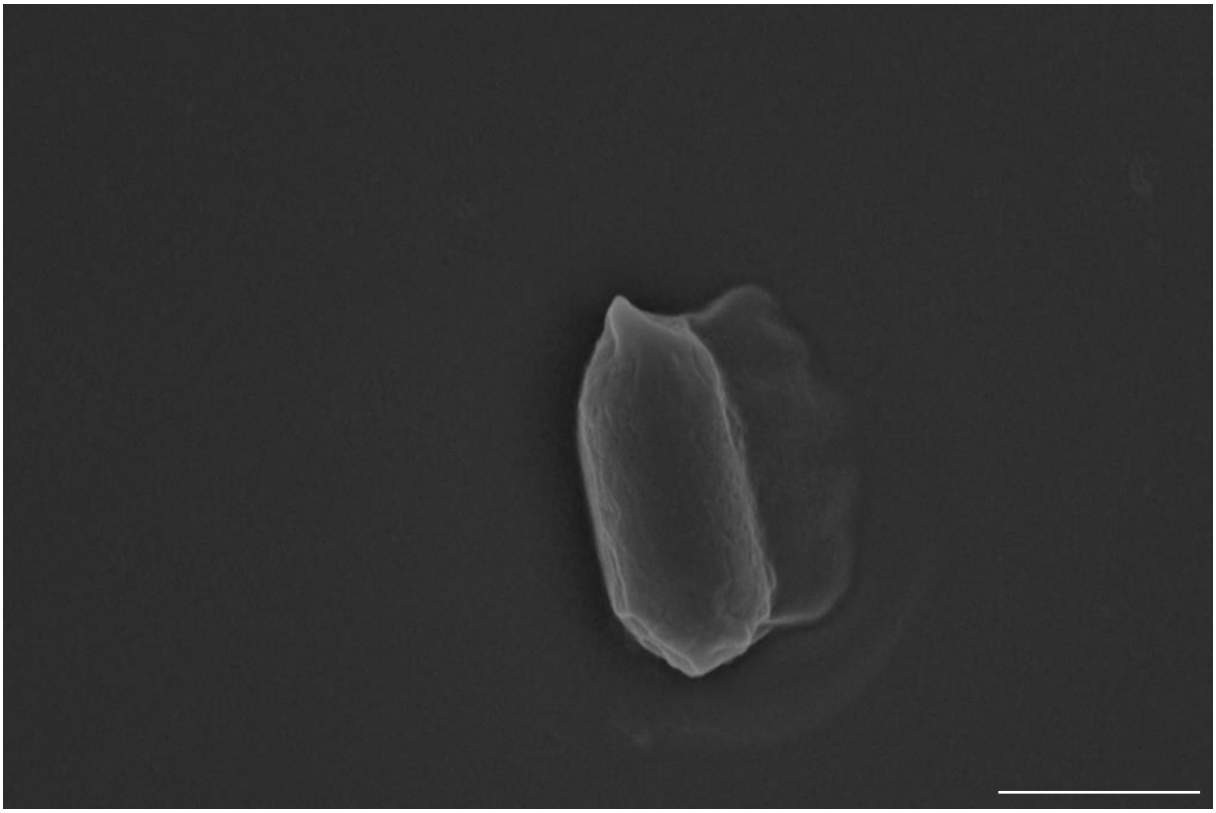

Figure S6. SEM micrograph of *C. difficile* spore. Scalebar is 1 µm.